Calculation of thermodynamic properties of small Lennard-Jones clusters incorporating anharmonicity

Jonathan P. K. Doye and David J. Wales
University Chemical Laboratories, Lensfield Road, Cambridge CB2 1EW, United Kingdom

(Received 12 January 1995; accepted 13 March 1995)

A method for calculating thermodynamic properties of clusters from knowledge of a sample of minima on the potential energy surface using a harmonic superposition approximation is extended to incorporate anharmonicity using Morse correction terms to the density of states. Anharmonicity parameters are found for different regions of the potential energy surface by fitting to simulation results using the short-time averaged temperature as an order parameter. The resulting analytical expression for the density of states can be used to calculate many thermodynamic properties in a variety of ensembles, which accurately reproduce simulation results. This method is illustrated for 13-atom and 55-atom Lennard-Jones clusters. © *1995 American Institute of Physics.*

I. INTRODUCTION

Before Monte Carlo (MC) and molecular dynamics (MD) simulations became computationally feasible, considerable attention was given to the calculation of thermodynamic properties of clusters from knowledge of the vibrational spectrum of a low energy structure using a harmonic approximation.[1–5] McGinty and Burton realized that if their results were to have relevance for more than low temperature behavior other configurations needed to be included in their partition function,[2–4] but without the means to systematically search the potential energy surface (PES) they were unable to implement this extension of their approach. The objective behind these studies was to get free energies in order to study homogeneous nucleation.

Once MC and MD simulations became feasible, work on the thermodynamics of clusters concentrated on obtaining thermodynamic information from the simulations, as the information gained is ''exact'' within the statistical errors of the simulation. In particular, it includes the thermodynamic effects of anharmonicity. This approach has been most successful. The multihistogram method[6,7] used by Labastie and Whetten extracts the configurational density of states from simulation.[8] Convolution with the kinetic energy density of states gives the total energy density of states, $\Omega(E)$, from which many other thermodynamic functions can be calculated. Labastie and Whetten applied the method to the first three icosahedral Lennard-Jones (LJ) clusters,[8] unequivocally showing that there are *S*-bends (or Van der Waals loops) in the microcanonical caloric curves of LJ_{55} and LJ_{147}. This method has since been used to calculate the complete phase diagram[9] for LJ_{55} and to investigate the melting transition for LJ_{13} and $(H_2O)_8$.[10] The multihistogram method obtains $\Omega(E)$ to within an unknown multiplicative factor, and this is sufficient for most applications. Weerasinghe and Amar used an adiabatic switching method to fix the absolute value of $\Omega(E)$, and subsequently used $\Omega(E)$ to calculate rates of evaporation of LJ clusters using phase space theory.[11]

Although numerically successful, the above approach gives little physical insight into the processes being simulated. Stillinger and Weber in their studies of bulk melting introduced the idea of ''inherent structures.''[12] Every configuration of a system can be mapped onto a minimum of the PES, an ''inherent structure,'' by a steepest-descent path or ''quench.'' This mapping allows the partition function to be separated into a term due to the energy spectrum of the inherent structures and a term due to thermal motion within the wells of the inherent structures. This approach can give much greater physical insight into a process such as melting, because the thermodynamics can be related to the structures of the minima on the PES. Similarly, an understanding of how the structure and topology of PES's differ can be used to explain differences in thermodynamic properties.

The success of Berry and co-workers in elucidating the melting of small Lennard-Jones clusters was partly based on their emphasis on understanding the thermodynamic and dynamic properties in relation to the qualitative features of the PES.[13,14] In particular they used systematic quenching to find the important low energy minima on the surface. This procedure has now become a standard tool in understanding the thermodynamics and dynamics of clusters and has been applied to LJ,[15] argon,[16] alkali halide,[17,18] metal,[19] water,[20] and C_{60} clusters.[21,22] Similarly, a knowledge of the transition states on the PES can provide a greater insight into the dynamics of a system.[23] This information was first obtained by the application of the eigenvector-following and ''slowest slides'' methods,[24] and has been used in combination with quenching to understand the melting dynamics of small LJ,[25] alkali halide,[17] metal,[19] water,[26] and C_{60} clusters.[21,22]

Bixon and Jortner[27] considered the effect of model energy spectra of the inherent structures on thermodynamic properties, in particular on the microcanonical and canonical caloric curves. They showed that a large energy gap between the global minimum and a manifold consisting of a large number of higher energy minima was necessary to produce a significant feature in the caloric curves.

Subsequently, we have developed an approach in which $\Omega(E)$ is directly calculated from knowledge of the PES.[28,29] A sample of minima is generated by systematic quenching from a high energy MD run. $\Omega(E)$ is then calculated by summing the harmonic density of states for each minima. This approach has been called the harmonic superposition method. It has been applied to LJ,[20,28] water,[20] and model metal clusters[19] to calculate the microcanonical caloric

curve, the heat capacity, the Helmholtz free energy, the canonical total energy distribution function,[19,20,28] Landau free energy barriers,[30] and thermodynamic properties for different regions of the PES, defined by a suitable order parameter.[31] Franke *et al.* have independently applied the same ideas to small LJ clusters.[32]

In Sec. II we briefly review the harmonic superposition method. In Sec. III we consider possible ways of including anharmonicity, and in Sec. IV we apply the resulting expressions for the density of states to calculate a variety of thermodynamic properties. LJ_{13} and LJ_{55} are used as examples to evaluate the effectiveness of the method. These are the two smallest icosahedral clusters and have been much studied theoretically because of their special stability.

II. THE HARMONIC SUPERPOSITION METHOD

The total energy density of states associated with a single minimum on the PES is, in the harmonic approximation,[13]

$$\Omega(E)=\frac{(E-E^0)^{\kappa-1}}{\Gamma(\kappa)\Pi_{j=1}^{\kappa}h\nu_j}\,\theta(E-E^0), \tag{1}$$

where E^0 is the potential energy of the minimum, θ is the Heaviside step function, and κ, the number of vibrational degrees of freedom, is $3N-6$. To calculate the density of states for the whole system, all the minima on the PES need to be considered. We make a superposition approximation and sum the density of states over all the minima low enough in energy to contribute. This approximation is equivalent to assuming that the phase space hyperellipsoids associated with each minimum do not overlap. This gives

$$\Omega(E)=\sum_{E_s^0<E}\frac{n_s^*(E-E_s^0)^{\kappa-1}}{\Gamma(\kappa)\Pi_{j=1}^{\kappa}h\nu_j^s}, \tag{2}$$

where the sum is over all the geometrically distinct minima on the surface; n_s^*, the number of permutational isomers of minimum s, is given by $n_s^*=2N!/h_s$, where h_s is the order of the point group of s.

The difficulty with Eq. (2) is that for all but the very smallest clusters this sum involves an impractically large number of minima. Hoare and McInnes,[33] and more recently Tsai and Jordan[34] have enumerated lower bounds to the number of geometric isomers for LJ clusters from 6 to 13 atoms. This number rises exponentially with N. Extrapolating this trend gives for LJ_{55} an estimate of 1×10^{21} geometric isomers. In such a case, as it is not possible to obtain a complete set of minima, a representative sample is needed. A large set of minima can be obtained by systematic quenching from a high energy MD trajectory. However, this gives a greater proportion of the low energy minima than of the high energy minima. Consequently, if the sample is used in Eq. (2) it is likely to underestimate the density of states due to the high energy minima, and so be inaccurate at high energies.

A method is needed which corrects for the incomplete nature of the sample of minima. This correction can be achieved by weighting the density of states for each known minimum by g_s, the number of minima of energy E_s^0 for which the minimum s is representative. Hence,

TABLE I. Details of the two samples of minima used for LJ_{55}. E' is measured with respect to the global minimum icosahedron.

E'/ϵ	Number of minima
A 64.7485	989
B 70.2485	1153

$$\Omega(E)=\sum_{E_s^0<E}\frac{g_s n_s^*(E-E_s^0)^{\kappa-1}}{\Gamma(\kappa)\Pi_{j=1}^{\kappa}h\nu_j^s}, \tag{3}$$

where the sum is now over a representative sample of minima. The effect of g_s can be incorporated by using the quench statistics.[28] If the system is ergodic and the MD run is performed at constant energy, the number of quenches to a minimum, γ, is assumed to be proportional to the density of states of the set of g_s minima, i.e., $\gamma(E')_s\propto g_s\Omega(E')_s$. Hence,

$$\Omega(E)\propto\sum_{E_s^0<E}\gamma(E')_s\frac{\Omega(E)_s}{\Omega(E')_s} \tag{4}$$

$$\propto\sum_{E_s^0<E}\gamma(E')_s\left(\frac{E-E_s^0}{E'-E_s^0}\right)^{\kappa-1}, \tag{5}$$

where E' is the energy of the MD run.

If all the low energy minima are known, the n^* formula will be accurate at low energies. Therefore, the proportionality constant in the above equation can be found by matching it to the low energy form of the n^* formula. For LJ_{13} and LJ_{55}, the term due to the icosahedron is dominant at low energies, and other terms in the sum can be neglected. Comparing the first terms of Eqs. (2) and (5) gives for the proportionality constant, c,

$$c=\frac{n_0^*(E'-E_0^0)^{\kappa-1}}{\gamma(E')_0\Gamma(\kappa)\Pi_{j=1}^{\kappa}h\nu_j^0}. \tag{6}$$

A critical test of these formulas for $\Omega(E)$ is the predicted microcanonical caloric curve, which for LJ_{55} has an S-bend.[8] Using the thermodynamic definition of the microcanonical temperature, T_μ,

$$\frac{1}{kT_\mu}=\left(\frac{\partial\ln\Omega}{\partial E}\right)_{N,V}=\frac{1}{\Omega}\left(\frac{\partial\Omega}{\partial E}\right)_{N,V}; \tag{7}$$

an expression for T_μ can be derived.[28] For LJ_{55} we have two samples of minima produced by systematic quenching,[28] details of which are given in Table I. Sample A is from a MD run at an energy in the upper end of the coexistence region, and B at an energy just into the liquidlike region. The results for samples A and B using the n^* and γ formulations[28] are given in Fig. 1. From this it can be seen the n^* formula fails badly, predicting only an inflection in the caloric curve which is too high in energy, because it underestimates the contribution to $\Omega(E)$ from the higher energy minima. The γ formula is much more successful, reproducing the S-bend at the observed energy.[35] That the harmonic superposition method produces a caloric curve with the correct features shows, as Bixon and Jortner suggested,[27] that the distribution of

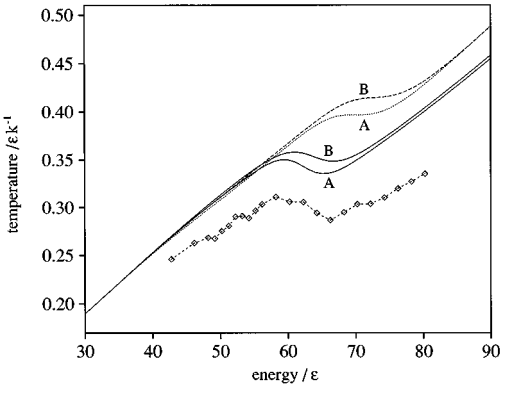

FIG. 1. Microcanonical caloric curves for LJ_{55}. The solid lines were calculated from the γ formula, the dashed lines were calculated from the n^* formula, and the dashed line with diamonds shows the simulation points. The sample of minima used in the calculations is marked on the graph. For details of the simulation see Ref. 31.

minima is critical in determining the form of the caloric curve. However, the S-bend is too shallow and lies at too high a temperature. The temperature difference is due to the harmonic approximation. The temperature rises linearly with energy for a single harmonic well. The anharmonic wells of the cluster, however, are flatter than the harmonic case especially around the transition state regions. Consequently, the cluster spends more time in these high potential energy, low temperature regions of the PES, and so the true temperature is lower than that given by the harmonic approximation.

For smaller clusters it was found that the performance of the n^* formula improved.[20] This improvement occurs because there are fewer minima on the PES of a smaller cluster and so the set of minima obtained from quenching is more complete.

The harmonic superposition method has three main possible sources of error. The first is from the systematic quenching and the resulting sample of minima and quench statistics. These errors can be mostly eliminated by having a long enough quench run to ensure ergodicity and choosing an appropriate energy for the run so that the relevant regions of phase space all have significant probabilities. When studying the thermodynamics of melting it is most appropriate to choose E' to lie in the coexistence region, as in the case of sample A, so that quenches to solidlike, liquidlike, and surface-melted states are frequent. The second possible source of error is the assumption that the phase volumes for each minima can be summed independently, i.e., the hyperellipsoids in phase space do not overlap. If they did the overlap would cause $\Omega(E)$ to be overestimated. Of course, above an energy threshold the true phase volumes of each minimum are interconnected, but this interconnection is normally due to the extension of the phase volumes due to anharmonicity to form necks in phase space along the transition state valleys. The third possible source of error is the harmonic approximation. Near the bottom of the well this is a reasonable assumption, but as the energy is increased some parts of the well become increasingly flat. Consequently the harmonic approximation causes $\Omega(E)$ to be underestimated. Comparison of the caloric curves from simulation and the harmonic superposition method (Fig. 1) shows that the harmonic superposition method does indeed underestimate $\Omega(E)$ and so the harmonic approximation is likely to be the main source of error.

III. ANHARMONICITY

Most attempts to model anharmonicity have concentrated on small systems. As the size of the system increases the difficulty increases greatly. For example, it would be impossible to do the necessary multidimensional phase space integrals in the definition of $\Omega(E)$,

$$\Omega(E)=\frac{1}{h^{\kappa}}\int\int \delta(H-E)dq^{\kappa}dp^{\kappa}. \tag{8}$$

Most approaches either attempt to calculate the anharmonic element using known information from the PES, such as the third and fourth derivatives of the potential at the minima and the dissociation energies[36] or assume the PES has a certain topology for which the partition function is known.[37–38] A normal mode approximation is often used because the multidimensional partition function is then the product of the one-dimensional normal mode partition functions. However, to obtain the density of states the partition function must be inverse Laplace transformed. This problem does not necessarily have an analytic solution, but there are a number of numerical methods.[39,40]

The only attempt that we know of to evaluate analytically the anharmonic density of states of clusters is due to Chekmarev and Umirzakov.[38] Their expression contained a number of unknown parameters, which they had to estimate. This approximate approach was partly due to their lack of information about the PES of LJ_{13}, the cluster they considered. They showed their form was able to produce the types of feature seen in the LJ_{13} caloric curve, if not to reproduce it accurately. The approach we use here is similar. We are looking for a relatively simple method that will provide an analytical expression for the anharmonic contribution to $\Omega(E)$. We also want to examine how far it is possible to use information extracted from the PES in this task. We will focus on LJ_{55} as a test of the methods developed. For LJ_{55} we have a sample of 3481 transition states which were found from a random selection of 402 of the minima in sample B defined above.[22] We have also calculated the analytical third derivatives for this potential.

A. The effect of transition state valleys

Transition states are crucial to the dynamics of a system, but how much effect do they have on the thermodynamics? Associated with a transition state is a flat valley on the PES which connects two minima. These transition state valleys will make a contribution to $\Omega(E)$. To consider their effect we need an expression for the density of states of a transition state valley.

We write the partition function for the transition state valley as a product of a vibrational partition function for the

$(\kappa-1)$ modes orthogonal to the transition vector and a translational partition function for motion along the transition state valley. This separation gives

$$Z_{\rm ts}=\frac{L}{h}\sqrt{\frac{2\pi m}{\beta}}\frac{e^{-\beta E_{\rm ts}}}{\Pi_{j=1}^{\kappa-1}\beta h\nu_j^{\rm ts}}, \tag{9}$$

where L is the length of the transition state valley. Inverse Laplace transforming this expression gives for the density of states of the transition state valley,

$$\Omega(E)_{\rm ts}=\frac{\sqrt{2\pi m}L(E-E_{\rm ts})^{\kappa-3/2}}{h^{\kappa}\Pi_{j=1}^{\kappa-1}\nu_j^{\rm ts}\Gamma(\kappa-1/2)}\,\theta(E-E_{\rm ts}). \tag{10}$$

Our expression for the total density of states is then

$$\Omega(E)=\sum_{E_s^0<E}\frac{n_s^*}{h^{\kappa}}\left[\frac{(E-E_s^0)^{\kappa-1}}{\Gamma(\kappa)\Pi_{j=1}^{\kappa}\nu_j^s}+\frac{\sqrt{2\pi m}}{\Gamma(\kappa-1/2)}\times\sum_{E_s^0+\Delta_{s,t}<E}\frac{\sigma_{s,t}L_{s,t}(E-E_s^0-\Delta_{s,t})^{\kappa-3/2}}{\Pi_{j=1}^{\kappa-1}\nu_j^{s,t}}\right], \tag{11}$$

where $\Delta_{s,t}$ is the barrier height of transition state t from minimum s, and the reaction path degeneracy $\sigma_{s,t}=h_s/h_t$ or $2h_s/h_t$ for nondegenerate and degenerate rearrangement mechanisms, respectively.[41] A degenerate transition state connects different permutational isomers of the same minimum. In the γ formulation we now have

$$\Omega(E)=\sum_{E_s^0<E}\gamma(E')_s\,\frac{(E-E_s^0)^{\kappa-1}/\Gamma(\kappa)\Pi_{j=1}^{\kappa}\nu_j^s+\sqrt{2\pi m}/\Gamma(\kappa-1/2)\Sigma_{E_s^0+\Delta_{s,t}<E}\sigma_{s,t}L_{s,t}(E-E_s^0-\Delta_{s,t})^{\kappa-3/2}/\Pi_{j=1}^{\kappa-1}\nu_j^{s,t}}{(E'-E_s^0)^{\kappa-1}/\Gamma(\kappa)\Pi_{j=1}^{\kappa}\nu_j^s+\sqrt{2\pi m}/\Gamma(\kappa-1/2)\Sigma_{E_s^0+\Delta_{s,t}<E'}\sigma_{s,t}L_{s,t}(E'-E_s^0-\Delta_{s,t})^{\kappa-3/2}/\Pi_{j=1}^{\kappa-1}\nu_j^{s,t}}. \tag{12}$$

Geometrically, the phase volume associated with the transition state valley is an elliptical hypercylinder. There is also a term due to the phase space overlap of this hypercylinder with the hyperellipsoid associated with the minimum. It can be evaluated,[42] however it is a small term and so we neglect it, especially as initially we are only trying to determine the magnitude of the effect of the transition state valleys.

The set of transition states previously calculated is not an exhaustive set for the sample of minima. Its incompleteness could cause an underestimation of the density of states arising from the transition state valleys. We therefore performed a more exhaustive search for transition states from 13 minima representing a wide range of energies. This search indicated that a reasonable estimate of the average number of low energy transition states per minimum was 20 (not counting permutational isomers). For each minimum the density of states of the known transition state valleys was multiplied by $20/n_{\rm ts}^s$, where $n_{\rm ts}^s$ is the number of known transition states for minimum s. If the sample of transition states contained none connected to a particular minimum, it was assigned 20 transition states with the average barrier height and average frequency. The length of the transition state valley was estimated using

$$L_{s,t}=D_{s,t}-\frac{1}{2\pi\overline{\nu^s}}\sqrt{\frac{2\Delta}{m}}, \tag{13}$$

where $D_{s,t}$ is the displacement in configuration space between minimum s and transition state t, and $\overline{\nu^s}$ is the geometric mean normal mode frequency of s. The second term is the geometric mean radius of the harmonic well in configuration space at an energy Δ above the minimum.

From the expression for $\Omega(E)$ in Eq. (12) the temperature can be calculated using Eq. (7). It can be seen from the microcanonical caloric curves given in Fig. 2(a) that the transition state valleys cause the caloric curve to bend away from the harmonic curve and the S-bend to be displaced downwards, but these effects are small. Even if the number of transition states connected to a minimum is assumed to be greater than 20 the effects are only slightly increased. The addition of the density of states of the transition state valleys only accounts for a small part of the difference between the harmonic and the true caloric curves. This result occurs not because the contribution of the transition state valleys to the density of states is small compared to that of the minima—in fact the transition state valleys make a larger contribution than the minima above about 55ϵ. Rather it occurs because the density of states for the transition state valleys is not very different from that of the minima; the valleys are modeled as harmonic in all but one dimension. We therefore conclude that a method of modeling the anharmonicity of the wells on the PES is needed to obtain an accurate $\Omega(E)$. This agrees with Stillinger and Stillinger's conclusion that intrawell anharmonicity is dominant for LJ_{55} because the caloric curve significantly deviates from the harmonic form at energies where the cluster always resides in the icosahedral well.[16]

B. The effect of well anharmonicity

Here we follow the method of Haarhoff[37,39] to calculate an anharmonic correction term to the density of states. The energy levels for a Morse oscillator are given by

$$E=\left(n+\frac{1}{2}\right)h\nu-\left(n+\frac{1}{2}\right)^2\frac{(h\nu)^2}{4D_e}. \tag{14}$$

This quadratic can be solved for n. The root corresponding to a bound state is

$$n+\frac{1}{2}=\frac{2D_e}{h\nu}\left(1-\sqrt{1-\frac{E}{D_e}}\right). \tag{15}$$

Assuming n is continuous and differentiating with respect to E gives a classical density of states,

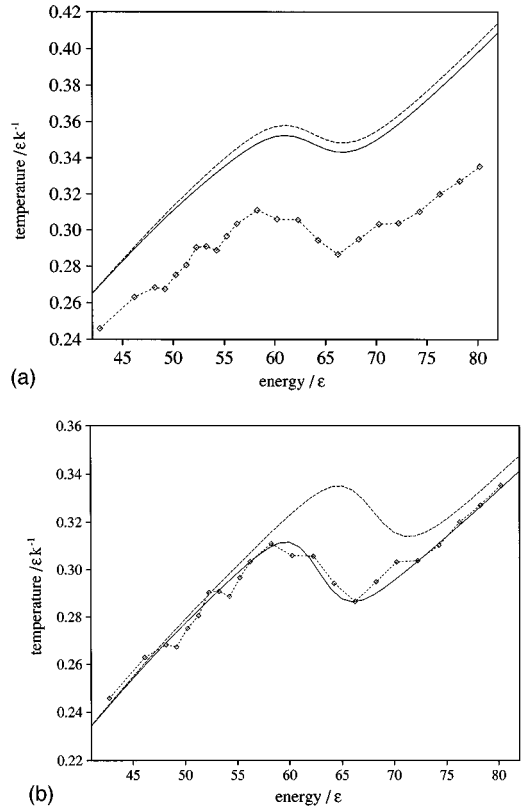

FIG. 2. Microcanonical caloric curves for LJ_{55} using (a) the γ formula with (solid line) and without (dashed line) the contribution from transition state valleys, and (b) using the γ formula including anharmonic terms with minima samples A (solid line) and B (dashed line). In both (a) and (b) the calculated caloric curves are compared to simulation (dashed line with diamonds).

$$\Omega(E)=\frac{dn}{dE}=\frac{1}{h\nu\sqrt{1-E/D_e}}=\frac{1}{h\nu}\left[1+\frac{E}{2D_e}+\frac{3}{8}\left(\frac{E}{D_e}\right)^2+\cdots\right], \tag{16}$$

where the square root has been expanded binomially. The expansion is valid if E/D_e is small. The first term in the series is the harmonic term. The full series will diverge as $E\rightarrow D_e$. This divergence is the correct behavior for the Morse oscillator, but for the case of a cluster isomerization $\Omega(E)$ remains finite as $E\rightarrow\Delta$ from below, where Δ is the barrier height. As we are seeking a correction term for well anharmonicity, it seems reasonable to truncate Eq. (16) and examine the effect of the first term in this series. Laplace transformation then gives for the partition function

$$z=\frac{1}{h\nu}\left(\frac{1}{\beta}+\frac{1}{2\Delta\beta^2}\right). \tag{17}$$

The multidimensional partition function is then

$$Z=\prod_{j=1}^{\kappa}\frac{1}{\beta h\nu_j}\left(1+\frac{1}{2\Delta_j\beta}\right). \tag{18}$$

Making the approximation that an average value of $1/\Delta$ can be used then gives

$$Z=\frac{1}{\Pi_{j=1}^{\kappa}h\nu_j}\sum_{l=0}^{\kappa}\frac{C_l^{\kappa}a^l}{\beta^{\kappa+l}}, \tag{19}$$

where $a=\langle 1/2\Delta\rangle$ is an anharmonicity parameter and C_l^{κ} is a binomial coefficient. Inverse Laplace transforming gives

$$\Omega(E)=\frac{1}{\Pi_{j=1}^{\kappa}h\nu_j}\sum_{l=0}^{\kappa}\frac{C_l^{\kappa}a^lE^{\kappa+l-1}}{\Gamma(\kappa+l)}. \tag{20}$$

The total density of states is found by summing over all the minima, giving

$$\Omega(E)=\sum_{E_s^0<E}\frac{n_s^*}{\Pi_{j=1}^{\kappa}h\nu_j^s}\sum_{l=0}^{\kappa}\frac{C_l^{\kappa}a_s^l(E-E_s^0)^{\kappa+l-1}}{\Gamma(\kappa+l)}. \tag{21}$$

Converting the above equation to the γ formulation using Eq. (4) gives

$$\Omega(E)\propto\sum_{E_s^0<E}\gamma(E')_s\left[\sum_{l=0}^{\kappa}\frac{C_l^{\kappa}a_s^l(E-E_s^0)^{\kappa+l-1}}{\Gamma(\kappa+l)}\Bigg/\sum_{l=0}^{\kappa}\frac{C_l^{\kappa}a_s^l(E'-E_s^0)^{\kappa+l-1}}{\Gamma(\kappa+l)}\right]. \tag{22}$$

The temperature follows from Eq. (7),

$$T_{\mu}=\frac{\Sigma_{E_s^0<E}\gamma(E')_s\left\{\Sigma_{l=0}^{\kappa}[C_l^{\kappa}a_s^l(E-E_s^0)^{\kappa+l-1}/\Gamma(\kappa+l)]\Big/\Sigma_{l=0}^{\kappa}[C_l^{\kappa}a_s^l(E'-E_s^0)^{\kappa+l-1}/\Gamma(\kappa+l)]\right\}}{k\Sigma_{E_s^0<E}\gamma(E')_s\left\{\Sigma_{l=0}^{\kappa}[C_l^{\kappa}a_s^l(E-E_s^0)^{\kappa+l-2}/\Gamma(\kappa+l-1)]\Big/\Sigma_{l=0}^{\kappa}[C_l^{\kappa}a_s^l(E'-E_s^0)^{\kappa+l-1}/\Gamma(\kappa+l)]\right\}}. \tag{23}$$

This anharmonic correction term has a similar form to that used by Chekmarev and Urmirzakov[38] but has been derived in a different way.

We consider two possible ways of calculating a_s from the potential energy surface of LJ_{55}. First, we consider using the third derivatives of the potential. The dissociation energy of a 1D Morse oscillator can be found from the second and third derivatives of the potential by

$$D_e=\frac{(V'')^3}{(V''')^2}. \tag{24}$$

If off-diagonal elements in the multidimensional case are ignored, the above equation can be used to calculate the barrier heights associated with each normal mode. Using analytical third derivatives of the LJ potential, the Cartesian third derivatives for the LJ_{55} icosahedron were calculated and transformed to obtain the diagonal elements in the Hessian eigenvector basis. This scheme underestimates the anharmonicity and gives values which when substituted into Eq. (22) have an insignificant effect on $\Omega(E)$, because the off-diagonal elements, which far outnumber the diagonal elements, should not be neglected. However, there is no obvious way to calculate the effect of the off-diagonal elements and for a system such as LJ_{55} the transformation of the third derivatives into the Hessian eigenvector basis is too computationally expensive for the off-diagonal elements.

The second method considered was to use the barrier heights of our transition state sample. An average barrier height was calculated for each minimum, but for some minima it led to a gross overestimation of the anharmonicity and unphysical caloric curves. The barrier heights are not a good quantitative measure of the anharmonicity of an individual minimum. This method was therefore not considered further.

Therefore, instead of trying to obtain a_s from the PES, we considered how it could be obtained by comparison with the simulation results. If a_s is taken to be independent of the energy of the minimum, then a value of a_s can be found which reproduces the S-bend in the caloric curve at the observed temperature and energy, but the temperature difference between the two turning points is still too small. However, one would expect the anharmonicity to depend upon the energy of the minimum; the higher energy minima are likely to have a greater anharmonicity than the solidlike minima.

In an accompanying paper[31] we have shown how thermodynamic properties can be calculated for different regions of the PES defined by a suitable order parameter by restricting the sum of Eq. (22) to minima in these regions. This procedure gives for T_i, the temperature of region i,

$$T_i=\frac{\Sigma_{E_s^0<E,s\in i}\gamma(E')_s\left\{\Sigma_{l=0}^{\kappa}[C_l^{\kappa}a_s^l(E-E_s^0)^{\kappa+l-1}/\Gamma(\kappa+l)]\right/\Sigma_{l=0}^{\kappa}[C_l^{\kappa}a_s^l(E'-E_s^0)^{\kappa+l-1}/\Gamma(\kappa+l)]\right\}}{k\Sigma_{E_s^0<E,s\in i}\gamma(E')_s\left\{\Sigma_{l=0}^{\kappa}[C_l^{\kappa}a_s^l(E-E_s^0)^{\kappa+l-2}/\Gamma(\kappa+l-1)]\right/\Sigma_{l=0}^{\kappa}[C_l^{\kappa}a_s^l(E'-E_s^0)^{\kappa+l-1}/\Gamma(\kappa+l)]\right\}}. \tag{25}$$

In the other paper the short-time averaged (STA) temperature is used as an order parameter to distinguish regions of the LJ_{55} PES, and it is shown that these regions are associated with minima in the different potential energy ranges given in Table II. Region I corresponds to the solidlike state, regions II and III to surface-melted states, and region VI to the liquidlike state. Consequently, the temperatures associated with the minima in the energy ranges I, II, III, and VI are known. Different values of the anharmonicity parameter, a_i, were therefore assigned to minima in the six different energy ranges. Values were chosen for regions I, II, III, and VI which reproduced the simulation results in Fig. 13 of Ref. 31. The caloric curves for each region accurately fitted the simulation curves showing that our anharmonic correction term has an appropriate form. Values of a_i for regions IV and V were chosen that were intermediate between the values for regions III and VI, but as these regions only make a small contribution to $\Omega(E)$ the exact value chosen will only have a very small effect on the overall caloric curve. The values of a_i are given in Table II. As would be expected the anharmonicity increases with the potential energy of the minima.

TABLE II. Partition of the minima of LJ_{55} into energy ranges and values of the anharmonicity parameter, a_i, for each range. Values for I, II, III, and VI were found by fitting the temperatures for these regions to the simulation results.

Region	Lower energy bound/ϵ	Higher energy bound/ϵ	a_i/ϵ^{-1}
I	−279.248 47	−279.248 47	0.50
II	−276.604 29	−276.199 35	0.51
III	−274.500 00	−273.000 00	0.53
IV	−273.000 00	−271.500 00	0.65
V	−271.500 00	−268.840 00	0.70
VI	−268.840 00	⋯	0.73

The microcanonical caloric curve was calculated using these values of a_i. Figure 2(b) shows that for sample A the calculated curve is in remarkable agreement with the simulation results. The calculated S-bend now has the correct depth, because the effect of the greater anharmonicity of the liquidlike state is to increase the difference in temperature between the two branches of the caloric curve. The success of this method can be understood from the equation

$$\frac{1}{T}=\sum_i \frac{p_i}{T_i}, \tag{26}$$

where p_i is the probability that the cluster is in region i. The probabilities at E', $p_i(E')$, are fixed by the quench frequencies,

$$p_i(E')=\frac{\Sigma_{s\in i}\gamma_s(E')}{\Sigma_s\gamma_s(E')}. \tag{27}$$

Furthermore, we show elsewhere that p_i calculated from sample A are in excellent agreement with simulation over a wide range of energy.[31] The values of a_i have been chosen to reproduce the simulation temperatures, T_i, and so the overall

temperature, T, is bound to be very accurate. Sample B produces worse results because there are fewer quenches to the solidlike and the surface-melted states, and so their quench frequencies are subject to larger statistical errors than for sample A.

For LJ_{13}, the STA temperature distribution is bimodal. The high temperature peak corresponds to solidlike clusters associated with the icosahedral global minimum, and the low temperature peak to liquidlike clusters. The residence times in the solidlike and liquidlike states are much shorter than for LJ_{55} and so the information provided by short-time averaging for LJ_{13} is less well-resolved. We partitioned the minima distribution into these two regions, and assigned values of a_i to each. The values of a_i were higher than for LJ_{55} and the curvature of the T_i curves differed from the simulation results. The apparently greater anharmonicity can be explained by the larger number of surface atoms for LJ_{13}. The incorrect curvature suggests that the energy dependence of the density of states is inappropriate and so the second-order Morse correction term to the density of states was included. The resulting T_i curves fitted the simulation results much more accurately. The partition function for a single minimum including this term is

$$Z=\prod_{j=1}^{\kappa}\frac{1}{\beta h\nu_j}\left[1+\frac{a}{\beta}+3\left(\frac{a}{\beta}\right)^2\right]^{\kappa}$$

$$=\frac{1}{\Pi_{j=1}^{\kappa}h\nu_j}\sum_{l=0}^{\kappa}\sum_{m=0}^{\kappa-l}D_{l,m}^{\kappa}\frac{3^m a^{l+2m}}{\beta^{\kappa+l+2m}}, \tag{28}$$

where

$$D_{l,m}^{\kappa}=\frac{\kappa!}{l!m!(\kappa-l-m)!}.$$

Inverse Laplace transforming and summing over all minima gives for the total density of states,

$$\Omega(E)=\sum_{E_s^0<E}\frac{n_s^*}{\Pi_{j=1}^{\kappa}h\nu_j^s}\sum_{l=0}^{\kappa}\sum_{m=0}^{\kappa-l}\times\frac{D_{l,m}^{\kappa}3^m a_s^{l+2m}(E-E_s^0)^{\kappa+l+2m-1}}{\Gamma(\kappa+l+2m)}. \tag{29}$$

In a MD simulation one calculates the kinetic temperature, T_K, from the kinetic energy, E_K, via the generalized equipartition theorem,

$$T_K=\frac{2\langle E_K\rangle}{k\kappa}. \tag{30}$$

This expression is exact in the canonical ensemble, but T_K differs by $\mathcal{O}(N^{-1})$ from the thermodynamic definition of temperature, Eq. (7), in the microcanonical ensemble.[43] For LJ_{55} the difference between the thermodynamic and kinetic temperatures is negligible. For LJ_{13} it is still small but not insignificant, and so T_K rather than T_μ is fitted to the simulation results. Bixon and Jortner found both temperatures produced very similar results in their model calculations of the microcanonical caloric curve.[27] T_K has been obtained for the superposition method by Franke *et al.* using the equipartition theorem,[32] however this method cannot be applied when anharmonicity is included. We obtain T_K through a different method. First, we note that

$$\langle E_K\rangle=\int_0^E p(E_K)E_K\,dE_K$$

$$=\frac{1}{\Omega(E)}\int_0^E E_K\Omega_c(E-E_K)\Omega_K(E_K)dE_K, \tag{31}$$

where $\Omega_K(E_K)$ is the kinetic density of states, $\Omega_c(E_c)$ is the configurational density of states, and the potential energy E_c is given by $E_c=E-E_K$. Deconvoluting $\Omega_K(E_K)$ from $\Omega(E)$ gives

$$\Omega_c(E_c)=\frac{1}{(2\pi m)^{\kappa/2}\Pi_{j=1}^{\kappa}\nu_j}\times\sum_{l=0}^{\kappa}\sum_{m=0}^{\kappa-l}\frac{D_{l,m}^{\kappa}3^m a_s^{l+2m}(E-E_s^0)^{\kappa/2+l+2m-1}}{\Gamma(\kappa/2+l+2m)}. \tag{32}$$

Integrating Eq. (31), summing over all minima and substituting into Eq. (30) gives

$$T_K=\frac{\Sigma_{E_s^0<E}\,n_s^*/\Pi_{j=1}^{\kappa}\,\nu_j^s\,\Sigma_{l=0}^{\kappa}\,\Sigma_{m=0}^{\kappa-l}\,D_{l,m}^{\kappa}\,3^m a_s^{l+2m}\,(E-E_s^0)^{\kappa+l+2m}/\Gamma(\kappa+l+2m+1)}{k\Sigma_{E_s^0<E}\,n_s^*/\Pi_{j=1}^{\kappa}\,\nu_j^s\,\Sigma_{l=0}^{\kappa}\,\Sigma_{m=0}^{\kappa-l}\,D_{l,m}^{\kappa}\,3^m a_s^{l+2m}\,(E-E_s^0)^{\kappa+l+2m-1}/\Gamma(\kappa+l+2m)}. \tag{33}$$

TABLE III. Details of the two samples of minima for LJ_{13}. E' is measured with respect to the global minimum icosahedron.

E'/ϵ	Number of minima
C 13.7768	95
D 18.3268	295

Sample C (Table III) was used to calculate the caloric curve of LJ_{13} for the γ formulation because it was produced from a MD run in the coexistence region and so should have more accurate quench statistics for the low energy minima, and sample D was used for the n^* formulation because it is from the liquidlike region and so has a larger sample of minima. The values of a_i assigned to solidlike and liquidlike clusters are given in Table IV. From Fig. 3 it can be seen that the caloric curve given by the n^* formulation agrees very well with simulation, because it is possible to obtain a near-complete set of minima for LJ_{13}. The γ formulation, however, has too high a transition temperature. This error arises

TABLE IV. Values of the anharmonicity parameter, a_i, for the solidlike (I) and liquidlike (II) regions of the PES. Region I is the potential well of the icosahedron and region II consists of all other minima.

Region	a_i/ϵ^{-1}
I	0.470
II	0.625

because the probability that the cluster is in the solidlike state derived from quenching is higher than the corresponding probability derived from the STA temperature distributions. In the γ formulation the probabilities, p_i, at E' are fixed by the quench statistics [Eq. (27)], and so this constraint leads to the higher transition temperature. The difference between the probabilities derived from quenching and the STA temperature distributions may be because there are regions of the PES which are in the basin of attraction of the icosahedron but which have thermodynamic properties similar to a liquidlike well, or because the short-time averaging does not distinguish between the solidlike and liquidlike states with the same resolution as for LJ_{55}. This difference does not stem from the quench method since we obtained similar quench statistics with steepest-descent,[44] conjugate gradient,[45] and eigenvector-following[46] methods.

IV. THERMODYNAMIC PROPERTIES

The accurate expressions for $\Omega(E)$ developed in the previous section can be used to give a wide range of thermodynamic functions, in fact, all except those that depend on derivatives of N or V. The exceptions arise because the thermodynamic properties of small clusters are discontinuously dependent on N and because the volume of a cluster is hard to define.[9] The formulas for the functions illustrated in this section are given in the Appendix. They have, for the most part, been derived in previous work within the harmonic approximation;[28,30] the extension to incorporate anharmonicity follows simply from the expressions given in Sec. III. The results are given for the most accurate partition functions; the first-order corrected γ formula for LJ_{55} and the second-order corrected n^* formula for LJ_{13}.

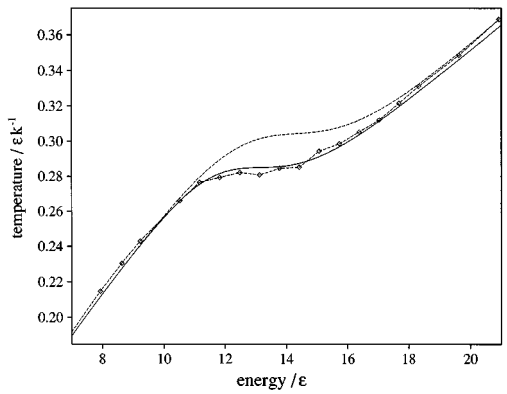

FIG. 3. Microcanonical caloric curves for LJ_{13} using the n^* formula (solid line), the γ formula (dashed line), and from simulation (dashed line with diamonds). Both the n^* and γ formula curves include anharmonic terms.

Harmonic and anharmonic results for the caloric curves, the heat capacity C_v, the Helmholtz free energy A, the transition temperature $T_{1/2}$, and the latent heat L_m are compared in Figs. 4 and 5 and Table V. We define $T_{1/2}$ as the temperature for which the two states have an equal Landau free energy, $F(E_c)$. L_m is the internal energy difference between the two states at $T_{1/2}$ and was obtained by extrapolating the caloric curves for each state to $T_{1/2}$ using Eq. (25). For LJ_{13}, this procedure simply gives $L_m = U_{\mathrm{II}} - U_{\mathrm{I}}$, where U_i is the internal energy of region i. For LJ_{55}, we have used $L_m = U_{\mathrm{V-VI}} - U_{\mathrm{I-IV}}$, where $U_{\mathrm{I-IV}}$ is the internal energy for the region of the PES formed from the combination of regions I–IV, and so L_m does not include the latent heat of surface-melting. Just integrating C_v over the transition region would overestimate L_m because it would also include the energy needed to raise the temperature of the cluster.

The anharmonic caloric curves are displaced downward and away from their harmonic equivalents because of the increased densities of states associated with higher potential energy, lower temperature regions of the PES. The anharmonic heat capacity curve of LJ_{55} is in very good agreement with results from the multihistogram MC method.[8] The peak in the heat capacity curve is larger and sharper when anharmonicity is included. This change can be understood by considering a two level system, which is a reasonable model to describe the equilibrium between solidlike and liquidlike states of the cluster. The partition function can be written as $Z = \Sigma_i Z_i$, where the sum is over the two distinct regions of phase space. It follows that

$$U = -\left(\frac{\partial \ln Z}{\partial \beta}\right)_{N,V} = -\frac{1}{Z}\sum_i \left(\frac{\partial Z_i}{\partial \beta}\right)_{N,V} = \sum_i p_i U_i, \tag{34}$$

where $p_i = Z_i/Z$ and $U_i = -(\partial \ln Z_i/\partial\beta)_{N,V}$. Hence,

$$C_v = \left(\frac{\partial U}{\partial T}\right)_{N,V} = \sum_i \left[p_i C_{v,i} + U_i\left(\frac{\partial p_i}{\partial T}\right)_{N,V}\right]$$
$$= \frac{1}{2}(C_{v,1} + C_{v,2}) + L_m\left(\frac{\partial p_2}{\partial T}\right)_{N,V} \quad \text{when} \quad p_1 = p_2 = \frac{1}{2}, \tag{35}$$

where $L_m = U_2(T_{1/2}) - U_1(T_{1/2})$ and $C_{v,i} = (\partial U_i/\partial T)_{N,V}$. As

$$\left(\frac{\partial p_i}{\partial T}\right)_{N,V} = \frac{1}{kT^2}\left[\frac{Z_i}{Z^2}\left(\frac{\partial Z}{\partial \beta}\right)_{N,V} - \frac{1}{Z}\left(\frac{\partial Z_i}{\partial \beta}\right)_{N,V}\right] = \frac{p_i}{kT^2}(U_i - U), \tag{36}$$

$$\left(\frac{\partial p_2}{\partial T}\right)_{N,V} = \frac{p_1 p_2}{kT^2}(U_2 - U_1) = \frac{L_m}{4kT_{1/2}^2} \quad \text{when} \quad p_1 = p_2 = \frac{1}{2}. \tag{37}$$

Substituting this result into Eq. (35) gives

$$C_v = \frac{1}{2}(C_{v,1} + C_{v,2}) + \frac{L_m^2}{4kT_{1/2}^2}. \tag{38}$$

The greater anharmonicity of liquidlike minima causes L_m to be larger when anharmonicity is included. This change has two effects; it increases the area under the heat capacity

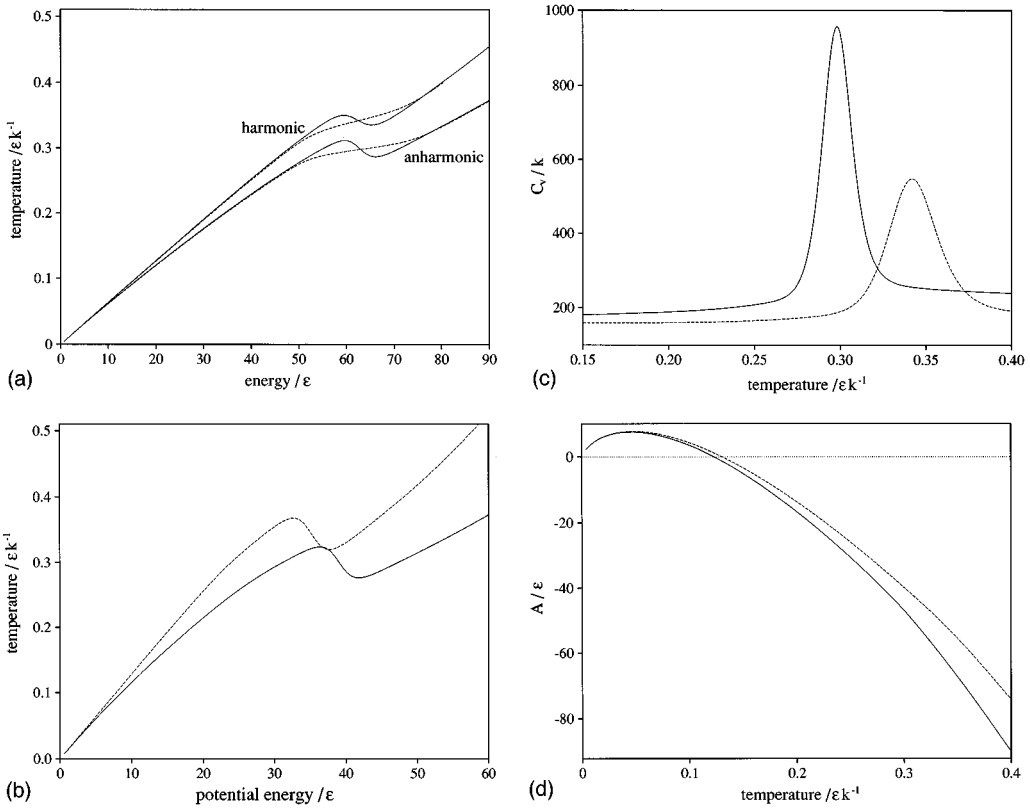

FIG. 4. Comparison of harmonic and anharmonic thermodynamic functions of LJ_{55}; (a) the microcanonical (solid line) and canonical (dashed line) caloric curves; (b) the isopotential caloric curve; (c) $C_v(T)$; and (d) $A(T)$. In all except (a) the anharmonic curve is denoted by a solid line and the harmonic by a dashed line. Energies are measured with respect to the global minimum icosahedron.

peak, and causes the cluster to change between the two states more rapidly with temperature, decreasing the width of the peak.

From Fig. 6 it can be seen that the probability of LJ_{55} being in a surface-melted state is lowest in the canonical ensemble and highest in the isopotential ensemble. This result is due to the dependence of the partition function on the independent variables, T, E, and E_c, of the three ensembles. In the canonical ensemble, Z is exponentially dependent on T, and is the most steeply varying of the three partition functions. In the microcanonical and isopotential ensembles, Ω and Ω_c are dependent on powers of E and E_c, respectively. As the exponent of E_c is lower than that for E, Ω_c is the slowest varying of the partition functions. For LJ_{55} $n_l/n_{sm} \gg n_{sm}/n_s$ (Table VI), where n_s, n_{sm}, and n_l are the number of minima in the solidlike, surface-melted, and liquidlike states. Consequently, as the partition function becomes more steeply varying, the surface-melted state is seen for a narrower range of the independent variable, i.e., the contribution of the liquidlike states overtakes the surface-melted states at an earlier stage in the surface-melting transition.

TABLE V. Transition temperatures and latent heats for LJ_{13} and LJ_{55}.

	LJ_{13}	LJ_{55}
$T_{1/2}/\epsilon k^{-1}$ (anharmonic)	0.2869	0.2985
$T_{1/2}/\epsilon k^{-1}$ (harmonic)	0.3512	0.3427
L_m/ϵ (anharmonic)	3.696	15.821
L_m/ϵ (harmonic)	2.887	12.837

The Landau free energy, $F(Q)$, is the free energy of a system for a particular value of an order parameter Q. It is defined by

$$F(Q) = A_c - kT \ln p_Q(Q), \tag{39}$$

where $p_Q(Q)$ is the canonical probability distribution of the order parameter. The presence of two minima in $F(Q)$ indicates that there are two thermodynamically stable states at this temperature. When E_c is used as an order parameter, simulations have shown that LJ_{55} has two Landau free energy minima which correspond to the solidlike and liquidlike states.[30] Bimodality in the canonical energy distribution function, $f(E)$, implies that there are two Landau free energy minima as a function of the order parameter, E. Figures 7 and 8 show that both LJ_{13} and LJ_{55} have a range of temperature for which two Landau free energy minima are observed. The predicted free energy curves for LJ_{55} are in very good agreement with simulation.[30] The solidlike and surface-melted states both contribute to the low energy minimum in

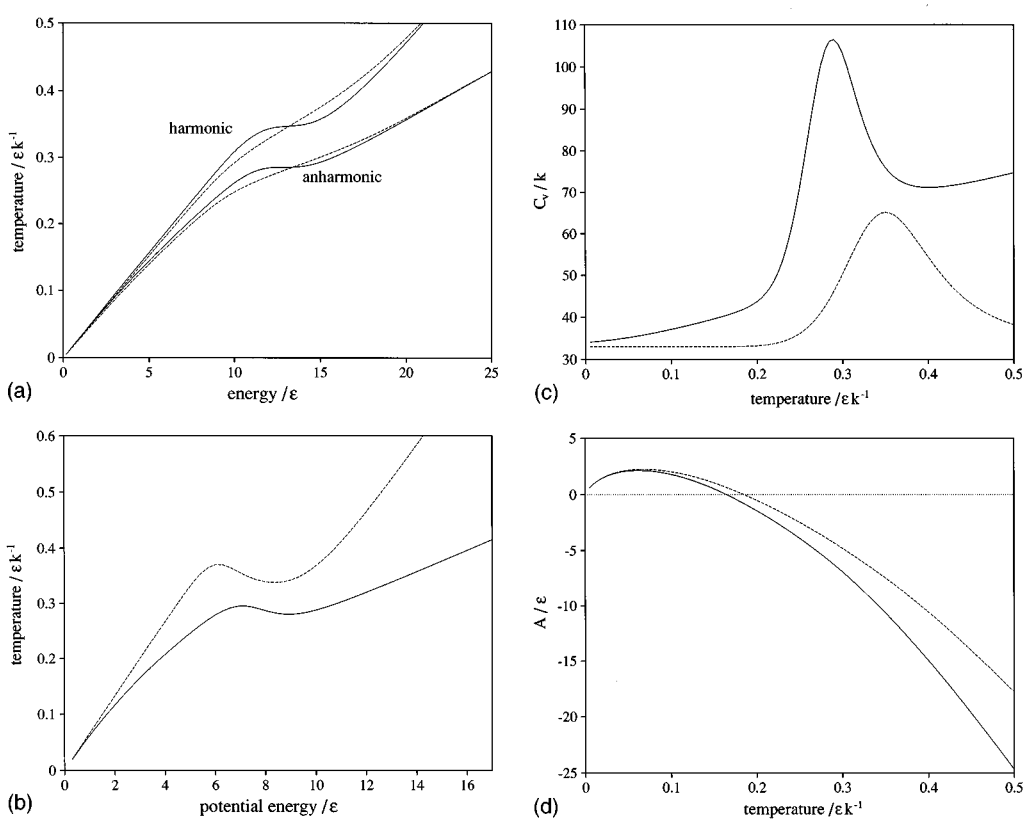

FIG. 5. Comparison of harmonic and anharmonic thermodynamic functions of LJ_{13}; (a) the microcanonical (solid line) and canonical (dashed line) caloric curves; (b) the isopotential caloric curve; (c) $C_v(T)$; and (d) $A(T)$. In all except (a) the anharmonic curve is denoted by a solid line and the harmonic by a dashed line. Energies are measured with respect to the global minimum icosahedron.

$F(E_c)$. For LJ_{13} the free energy barrier is much smaller and has not been observed in simulations. This may be because only three temperatures were tested in the simulations, the barrier is too small to be detected by simulation or the barrier is an artifact of inaccuracies in our analytical partition function.

The turning points in $F(E_c)$ and $f(E)$ correspond to points on the isopotential and the microcanonical caloric curves, respectively. This can be demonstrated for $F(E_c)$ by solving the equation $(\partial F/\partial E_c)_{N,V}=0$. The solution is $1/kT=(\partial \ln \Omega_c/\partial E_c)_{N,V}$, which is simply the definition of the isopotential temperature. The maxima in $F(E_c)$ correspond to the segment of the caloric curve with negative slope, and the minima to segments with positive slope. Therefore the temperature range for which $F(E_c)$ has two minima is the same as the depth of the S-bend in the isopotential caloric curve, as can be seen from Figs. 4(b) and 7(c), and 5(b) and 8(b).

Comparing the results for LJ_{13} and LJ_{55} we see that the effects of size are apparent. For LJ_{55} the melting transition is much more pronounced; it has a sharper peak in C_v, more pronounced S-bends in the microcanonical and isopotential caloric curves, a larger Landau Free energy barrier, a larger temperature range for which solidlike and liquidlike clusters coexist, a larger latent heat per atom, and a higher melting temperature. This behavior is closer to the first-order phase transition of bulk matter.

Estimates of the number of minima in different regions of the PES can be obtained from the quench frequencies. Using Eqs. (3), (4), and (6) an expression for g_s can be derived,

$$g_s=\frac{\gamma(E')_s h_s \Pi_{j=1}^{\kappa}\nu_j^s}{\gamma(E')_0 h_0 \Pi_{j=1}^{\kappa}\nu_j^0}\sum_{l=0}^{\kappa}\frac{C_l^{\kappa}a_0^l(E'-E_0^0)^{\kappa+l-1}}{\Gamma(\kappa+l)}\Bigg/\sum_{l=0}^{\kappa}\frac{C_l^{\kappa}a_s^l(E'-E_s^0)^{\kappa+l-1}}{\Gamma(\kappa+l)}. \tag{40}$$

From g_s, the sum $[G_m(E)]$ and associated energy density of states $[\Omega_m(E)]$ of geometrically distinct minima can be calculated using

$$G_m(E)=\sum_{E_s^0<E} g_s \quad \text{and} \quad \Omega_m(E)=\frac{dG_m}{dE}. \tag{41}$$

This approach has been applied to LJ_{55}. From Fig. 9 it can be seen that the number of minima for LJ_{55} rises exponentially with the energy. The total number of minima in the energy range probed by the MD quenching (potential energies up to -259ϵ) is 8.3×10^{11}. This is much less than the total number of minima predicted by extrapolating Tsai and Jordan's results and so suggests that the number of minima will continue to rise exponentially above -259ϵ. The present method

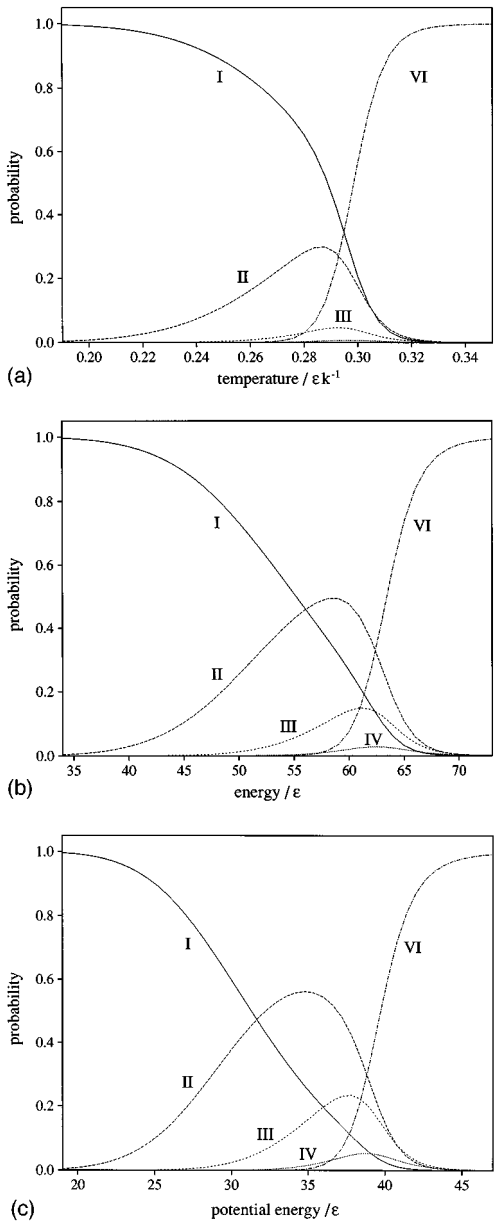

FIG. 6. Probabilities of LJ_{55} being in regions I, II, III, IV, and VI of the PES for (a) canonical, (b) microcanonical, and (c) isopotential ensembles.

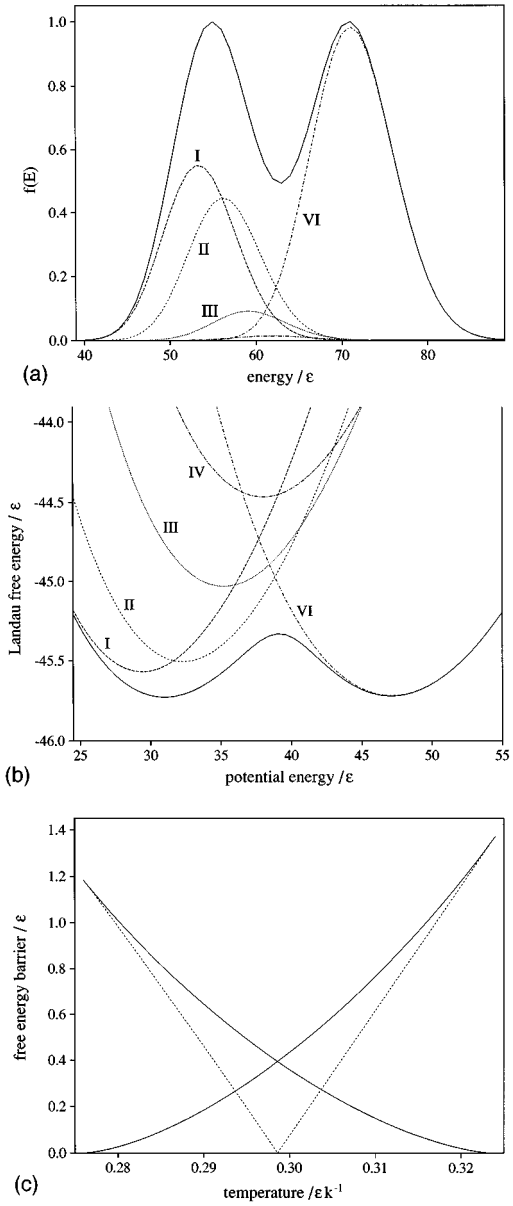

FIG. 7. Plots for LJ_{55} of (a) $f(E)$ at $T=0.2985$, (b) $F(E_c)$ at $T=0.2985$, and (c) the free energy barrier heights (solid lines) and the free energy difference between solidlike and liquidlike states (dashed line) for $F(E_c)$. In (a) and (b) the contributions of the different regions of the PES are also indicated.

TABLE VI. Estimated numbers of geometrically distinct minima of LJ_{55} in the six energy ranges given in Table II calculated from the quench frequencies for sample A.

	Number of minima	
Region	anharmonic	harmonic
I	1	1
II	11.3	6.3
III	994.6	457.9
IV	81.5	2871.2
V	1.26×10^{5}	1.22×10^{6}
VI	8.30×10^{11}	3.11×10^{12}

can also be used to estimate the number of minima in the energy ranges I–VI (Table VI). The number of minima in range II is known[16] to be 11. The results from the quench frequencies agree well with this figure.

V. CONCLUSIONS

Accurate analytic expressions for the density of states that include anharmonicity have been produced for LJ_{13} and LJ_{55}, which primarily use information obtained from the potential energy surface. From these expressions, many thermodynamic properties can be calculated. The analytical results accurately reproduce values obtained from simulation,

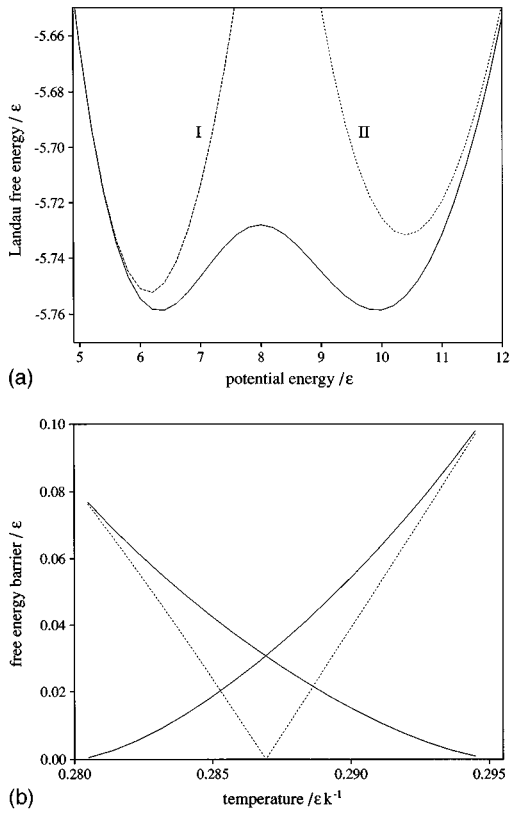

FIG. 8. Plots for LJ_{13} of (a) $F(E_c)$ at $T=0.2869$, and (b) the free energy barrier heights (solid lines) and the free energy difference between solidlike and liquidlike states (dashed line) for $F(E_c)$. In (a) the contributions of liquidlike and solidlike states are shown.

and give greater physical insight into the thermodynamics by allowing the roles of different parts of the PES to be analyzed. An alternative approach in which the partition function was corrected by allowing for transition state valleys showed little improvement from the original harmonic superposition approximation. The methods developed here should be applicable to other types of clusters, although, as in our examples, the form of the anharmonic terms would probably depend on the type and size of cluster considered. They could also, in principle, be applied to periodic models of bulk matter. However, there would then be the added difficulty that the PES, and consequently the minima on the PES, will depend on the pressure. The expressions for the density of states could also be used to calculate accurate rate constants using RRKM theory,[17,39] and so aid quantitative elucidation of dynamic properties from a knowledge of the transition states on the PES.

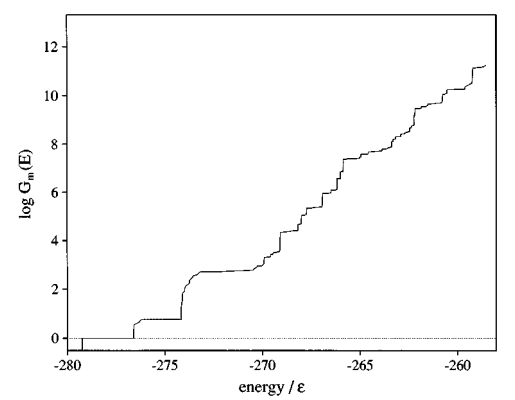

FIG. 9. Plot of $G_m(E)$ for LJ_{55} as a function of the potential energy of the minimum calculated from the quench frequencies of sample A.

ACKNOWLEDGMENTS

J. P. K. D. is grateful to the EPSRC for financial support and D. J. W. is a Royal Society Research Fellow.

APPENDIX

In this Appendix, the formulas for some of the thermodynamic quantities that can be calculated by the superposition method are given. The thermodynamic functions are derived from the following definitions.

In the isopotential ensemble,

$$p_i(E_c)=\frac{\Omega_{c,i}(E_c)}{\Omega_c(E_c)}, \quad \frac{1}{kT_c(E_c)}=\left(\frac{\partial \ln \Omega_c}{\partial E_c}\right)_{N,V}. \tag{A1}$$

In the microcanonical ensemble,

$$p_i(E)=\frac{\Omega_i(E)}{\Omega(E)}. \tag{A2}$$

In the canonical ensemble,

$$p_i(T)=\frac{Z_i}{Z},$$

$$U(T)=-\left(\frac{\partial \ln Z}{\partial \beta}\right)_{N,V}=\frac{1}{Z_{0,0}}(Z_{1,0}+Z_{0,1}),$$

$$C_v(T)=\left(\frac{\partial U}{\partial T}\right)_{N,V},$$

$$=\frac{1}{kT^2}\left[\frac{1}{Z_{0,0}}(Z_{2,0}+2Z_{1,1}+Z_{0,2})-\left(\frac{Z_{1,0}+Z_{0,1}}{Z_{0,0}}\right)^2\right], \tag{A3}$$

$$A(T)=E_0^0-kT \ln Z,$$

$$f(E)=\Omega(E)\exp(-\beta E),$$

$$F(E_c)=E_c-kT \ln \Omega_c(E_c),$$

where in $Z_{\alpha,\delta}$ the derivative of the exponential function of β in Z has been taken α times and the derivative of the inverse power of β in Z δ times. Therefore, $Z=Z_{0,0}$.

Below, we give the thermodynamic functions for the γ formulation with a first-order anharmonic correction which was used for LJ_{55},

$$T_c(E_c)=\frac{\Sigma_{E_s^0<E_c}\gamma(E')_s\Sigma_{l=0}^{\kappa}[C_l^{\kappa}a_s^l(E_c-E_s^0)^{\kappa/2+l-1}/\Gamma(\kappa/2+l)]\Big/\Sigma_{l=0}^{\kappa}[C_l^{\kappa}a_s^l(E'-E_s^0)^{\kappa+l-1}/\Gamma(\kappa+l)]}{k\Sigma_{E_s^0<E_c}\gamma(E')_s\Sigma_{l=0}^{\kappa}[C_l^{\kappa}a_s^l(E_c-E_s^0)^{\kappa/2+l-2}/\Gamma(\kappa/2+l-1)]\Big/\Sigma_{l=0}^{\kappa}[C_l^{\kappa}a_s^l(E'-E_s^0)^{\kappa+l-1}/\Gamma(\kappa+l)]},$$

$$Z_{\alpha,\delta}=c\sum_s \gamma(E')_s(E_s^0)^{\alpha}e^{-\beta E_s^0}\sum_{l=0}^{\kappa}\frac{\Gamma(\kappa+l+\delta)}{\Gamma(\kappa+l)}\frac{C_l^{\kappa}a_s^l}{\beta^{\kappa+l+\delta}}\Big/\sum_{l=0}^{\kappa}\frac{C_l^{\kappa}a_s^l(E'-E_s^0)^{\kappa+l-1}}{\Gamma(\kappa+l)}, \tag{A4}$$

$$F(E_c)=E_c-\frac{1}{\beta}\ln\frac{c}{\beta^{\kappa/2}}\sum_{E_s^0<E_c}\gamma(E')_s\sum_{l=0}^{\kappa}\frac{C_l^{\kappa}a_s^l(E_c-E_s^0)^{\kappa/2+l-1}}{\Gamma(\kappa/2+l)}\Big/\sum_{l=0}^{\kappa}\frac{C_l^{\kappa}a_s^l(E'-E_s^0)^{\kappa+l-1}}{\Gamma(\kappa+l)},$$

where

$$c=\frac{n_0^*}{\gamma(E')_0\Pi_{j=1}^{\kappa}h\nu_j^0}\sum_{l=0}^{\kappa}\frac{C_l^{\kappa}a_0^l(E'-E_0^0)^{\kappa+l-1}}{\Gamma(\kappa+l)}.$$

The harmonic forms can be recovered by taking the $l=0$ term. We obtain the n^* formulation by replacing

$$c\,\gamma(E')_s\Big/\sum_{l=0}^{\kappa}\frac{C_l^{\kappa}a_s^l(E'-E_s^0)^{\kappa+l-1}}{\Gamma(\kappa+l)}\ \text{ with }\ \frac{n_s^*}{\Pi_{j=1}^{\kappa}h\nu_j^s}. \tag{A5}$$

Below, we give the thermodynamic functions for the n^* formulation with second-order anharmonic corrections which was used for LJ_{13},

$$T_c(E_c)=\frac{\Sigma_{E_s^0<E_c}(n_s^*/\Pi_{j=1}^{\kappa}h\nu_j^s)\,\Sigma_{l=0}^{\kappa}\,\Sigma_{m=0}^{\kappa-l}[D_{l,m}^{\kappa}\,3^m a_s^{l+2m}(E_c-E_s^0)^{\kappa/2+l+2m-1}/\Gamma(\kappa/2+l+2m)]}{k\Sigma_{E_s^0<E_c}(n_s^*/\Pi_{j=1}^{\kappa}h\nu_j^s)\,\Sigma_{l=0}^{\kappa}\,\Sigma_{m=0}^{\kappa-l}[D_{l,m}^{\kappa}\,3^m a_s^{l+2m}(E_c-E_s^0)^{\kappa/2+l+2m-2}/\Gamma(\kappa/2+l+2m-1)]},$$

$$Z_{\alpha,\delta}=\sum_s\frac{n_s^*e^{-\beta E_s^0}(E_s^0)^{\alpha}}{\Pi_{j=1}^{\kappa}h\nu_j^s}\sum_{l=0}^{\kappa}\sum_{m=0}^{\kappa-l}\frac{\Gamma(\kappa+l+2m+\delta)}{\Gamma(\kappa+l+2m)}\frac{D_{l,m}^{\kappa}3^m a_s^{l+2m}}{\beta^{\kappa+l+2m+\delta}}, \tag{A6}$$

$$F(E_c)=E_c-\frac{1}{\beta}\ln\sum_{E_s^0<E_c}\frac{n_s^*}{\beta^{\kappa/2}\Pi_{j=1}^{\kappa}h\nu_j^s}\sum_{l=0}^{\kappa}\sum_{m=0}^{\kappa-l}\frac{D_{l,m}^{\kappa}3^m a_s^{l+2m}(E_c-E_s^0)^{\kappa/2+l+2m-1}}{\Gamma(\kappa/2+l+2m)}.$$

The harmonic forms can be recovered by taking the $l=0$, $m=0$ term, and the first order correction forms by taking the $m=0$ terms. We obtain the γ formulation by replacing

$$\frac{n_s^*}{\Pi_{j=1}^{\kappa}h\nu_j^s}\ \text{ with }\ c\,\gamma(E')_s\Big/\sum_{l=0}^{\kappa}\sum_{m=0}^{\kappa-l}\frac{D_{l,m}^{\kappa}3^m a_s^{l+2m}(E'-E_s^0)^{\kappa+l+2m-1}}{\Gamma(\kappa+l+2m)},$$

where

$$c=\frac{n_0^*}{\gamma(E')_0\Pi_{j=1}^{\kappa}h\nu_j^0}\sum_{l=0}^{\kappa}\sum_{m=0}^{\kappa-l}\frac{D_{l,m}^{\kappa}3^m a_0^{l+2m}(E'-E_0^0)^{\kappa+l+2m-1}}{\Gamma(\kappa+l+2m)}. \tag{A7}$$

[1] J. J. Burton, J. Chem. Phys. **52**, 345 (1970).
[2] D. J. McGinty, J. Chem. Phys. **55**, 580 (1971).
[3] J. J. Burton, J. Chem. Soc. Faraday II **69**, 540 (1972).
[4] J. J. Burton, J. Chem. Phys. **56**, 3123 (1972).
[5] W. G. Hoover, A. C. Hindmarsh, and B. L. Holian, J. Chem. Phys. **57**, 1980 (1972).
[6] I. R. McDonald, J. Chem. Soc. Faraday Discuss. **43**, 40 (1967).
[7] A. M. Ferrenberg and R. H. Swendsen, Phys. Rev. Lett. **63**, 1195 (1989).
[8] P. Labastie and R. L. Whetten, Phys. Rev. Lett. **65**, 1567 (1990).
[9] H.-P. Cheng, X. Li, R. L. Whetten, and R. S. Berry, Phys. Rev. A **46**, 791 (1992).
[10] C. J. Tsai and K. D. Jordan, J. Chem. Phys. **99**, 6957 (1993).
[11] S. Weerasinghe and F. G. Amar, J. Chem. Phys. **98**, 4967 (1993).
[12] F. H. Stillinger and T. A. Weber, Kinam A **3**, 159 (1981); Phys. Rev. A **25**, 978 (1982); J. Phys. Chem. **87**, 2833 (1983); J. Chem. Phys. **81**, 5089 (1984).
[13] F. G. Amar and R. S. Berry, J. Chem. Phys. **85**, 5943 (1986).
[14] T. L. Beck and R. S. Berry, J. Chem. Phys. **84**, 2783 (1986).
[15] J. D. Honeycutt and H. C. Andersen, J. Phys. Chem. **91**, 4950 (1987).
[16] F. H. Stillinger and D. K. Stillinger, J. Chem. Phys. **93**, 6013 (1990).
[17] J. P. Rose and R. S. Berry, J. Chem. Phys. **96**, 517 (1991).
[18] J. P. Rose and R. S. Berry, J. Chem. Phys. **98**, 3246 (1993).
[19] J. Uppenbrink and D. J. Wales, Z. Phys. D **26**, 258 (1993); J. Chem. Phys. **98**, 5270 (1993).

[20] D. J. Wales and I. Ohmine, J. Chem. Phys. **98**, 7245 (1993).
[21] D. J. Wales, J. Chem. Soc. Faraday Trans. **90**, 1061 (1994).
[22] D. J. Wales, J. Chem. Phys. **101**, 3750 (1994).
[23] R. S. Berry, Chem. Rev. **93**, 2379 (1993).
[24] D. J. Wales, J. Chem. Phys. **91**, 7002 (1989); H. L. Davis, D. J. Wales, and R. S. Berry, *ibid*. **92**, 4308 (1990).
[25] D. J. Wales and R. S. Berry, J. Chem. Phys. **92**, 4283 (1990).
[26] D. J. Wales and I. Ohmine, J. Chem. Phys. **98**, 7257 (1993).
[27] M. Bixon and J. Jortner, J. Chem. Phys. **91**, 1631 (1989).
[28] D. J. Wales, Mol. Phys. **78**, 151 (1993).
[29] D. J. Wales, Z. Phys. D **26**, 105 (1993).
[30] R. M. Lynden-Bell and D. J. Wales, J. Chem. Phys. **101**, 1460 (1994).
[31] J. P. K. Doye and D. J. Wales, J. Chem. Phys. **102**, 9673 (1995).
[32] G. Franke, E. R. Hilf, and P. Borrmann, J. Chem. Phys. **98**, 3496 (1993).
[33] M. R. Hoare and J. McInnes, J. Chem. Soc. Faraday Discuss. **61**, 12 (1976).
[34] C. J. Tsai and K. D. Jordan, J. Phys. Chem. **97**, 11 227 (1993).
[35] In Ref. 8, the energy scales of Figs. 1 and 2 are inconsistent, probably because $\Omega_c(E_c)$ was plotted, not $\Omega(E)$ as stated. Consequently, in Refs. 20 and 28 the energy of the *S*-bend and the bimodal $f(E)$ predicted by the harmonic superposition method were thought to be at a higher energy than observed by simulation.
[36] A. D. Isaacson and D. G. Truhlar, J. Chem. Phys. **80**, 2888 (1984).
[37] P. C. Haarhoff, Mol. Phys. **7**, 101 (1963).
[38] S. F. Chekmarev and I. H. Umirzakov, Z. Phys. D **26**, 373 (1993).
[39] W. Forst, *Theory of Unimolecular Reactions* (Academic, New York, 1973), Chap. 6.
[40] D. Romanini and K. K. Lehmann, J. Chem. Phys. **98**, 6437 (1993).
[41] A. J. Karas, R. G. Gilbert, and M. A. Collins, Chem. Phys. Lett. **193**, 181 (1992).
[42] J. P. K. Doye, CPGS thesis, University of Cambridge, 1994.
[43] M. P. Allen, and D. J. Tildesley, *The Computer Simulation of Liquids* (Clarendon, Oxford, 1987).
[44] M. Page and J. W. McIver, J. Chem. Phys. **88**, 922 (1988); M. Page, C. Doubleday, and J. W. McIver, *ibid*. **93**, 5634 (1990).
[45] W. H. Press, B. P. Flannery, S. A. Teukolsky, and W. T. Vetterling, *Numerical Recipes* (Cambridge University, Cambridge, 1986).
[46] D. J. Wales, J. Chem. Soc. Faraday Trans. **89**, 1305 (1993).